ACS EARTH AND SPACE CHEMISTRY

Article

Cite This: ACS Earth Space Chem. 2019, 3, 2623−2634

http://pubs.acs.org/journal/aesccq

Manganese Oxide Catalyzed Hydrolysis of Polyphosphates

Biao Wan,[†] Rixiang Huang,[†] Julia M. Diaz,[‡,#] and Yuanzhi Tang*[,†]

[†]School of Earth and Atmospheric Sciences, Georgia Institute of Technology, Atlanta, Georgia 30332-0340, United States

[‡]Department of Marine Sciences, Skidaway Institute of Oceanography, University of Georgia, Savannah, Georgia 31411, United States

Supporting Information

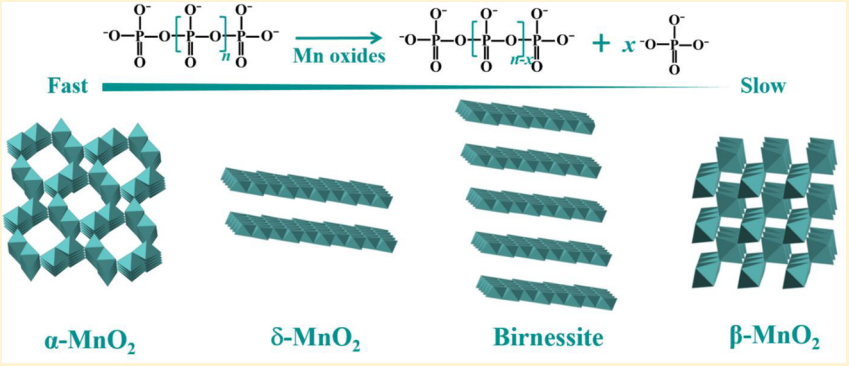

ABSTRACT: Polyphosphate (polyP) is a group of important phosphorus (P) species that plays critical roles in the marine P cycle and potentially mediates phosphorus (P) burial in sediments. Revealing the transformation of polyP is important for understanding the P cycle in aquatic environments. This study systematically investigated the hydrolysis of polyP with different chain lengths by four representative types of manganese (Mn) oxides (α-MnO_2, β-MnO_2, δ-MnO_2, and birnessite) under varied solution conditions. All four Mn oxides can rapidly hydrolyze polyP, with the hydrolysis rate in the order of α-MnO_2 > δ-MnO_2 > birnessite > β-MnO_2. The hydrolysis rates for longer chained polyP were relatively higher than those of shorter chained ones. Results from kinetic studies and time-resolved ^{31}P solution nuclear magnetic resonance (NMR) spectroscopy indicated that the reaction mechanism was through a terminal-only hydrolysis pathway via one-by-one cleavage of terminal P−O−P bonds. The presence of Ca^{2+} obviously enhanced both the hydrolysis rate and extent. The presence of other common metal cations (Mg^{2+}, Cu^{2+}, Zn^{2+}, and Mn^{2+}) also showed promotion on polyP hydrolysis by δ-MnO_2. Formation of cation-polyP ternary surface complexes is likely the dominant mechanism of cation promotion on polyP hydrolysis on Mn oxides. P K-edge X-ray absorption near edge structure (XANES) analysis indicated that solid calcium polyphosphate (Ca-polyP) granules can be hydrolyzed by α-MnO_2 and transformed into amorphous calcium phosphate (ACP) phase, with increasing ACP content as pH increased. This study highlights the rapid transformation of polyP at the mineral−water interface, and has significant implications for the alteration of P bioavailability in aquatic environments and for P burial in marine sediments.

KEYWORDS: *Mn oxides, polyphosphate, hydrolysis, adsorption, metal cations*

INTRODUCTION

Phosphorus (P) is an essential nutrient for all life. Numerous research efforts have been devoted to exploring P biogeochemical behaviors at mineral−water interfaces in both terrestrial and marine systems, which control the mobility, transformation, and bioavailability of P.[1,2] Polyphosphate (polyP) is an important group of phosphate-containing species, containing more than two phosphate (PO_4) groups joined by phosphoanhydride (P−O−P) bonds. PolyP can occur in ring and branched structures, although the linear structure is the most common form in nature.[3,4] PolyP is found in a wide range of environments and represents 1−13% of total P in planktonic organisms,[5,6] the dissolved and particulate pools of seawater,[7,8] marine sediments,[9] 1.5−11.4% of total P in lake sediments[10] and 0.4−7% of total P in soils.[11] A portion of the biologically internal polyP is released to aquatic environments during common cell events such as extracellular release, lysis, and death, thereby becoming biologically external.[12] As a result, substantial levels of polyP are routinely detected in both dissolved and particulate fractions of lakes, seawater, and the corresponding sediments.[9,10,12,13] Additionally, polyP compounds are important industrial chemicals, frequently used as reagents for water treatment, medicine, fertilizers, flame retardants, and food additives.[14] The widespread industrial applications of polyP can ultimately lead to their release into

Received: August 8, 2019
Revised: September 27, 2019
Accepted: October 21, 2019
Published: October 21, 2019

DOI: 10.1021/acsearthspacechem.9b00220
ACS Earth Space Chem. 2019, 3, 2623−2634

soils, water bodies, and sediments. The cycling of polyP in aquatic environments, which is strongly controlled by its interfacial biogeochemical behaviors (such as those involving mineral−water interfaces), is an important component of the global P cycle.[15]

Despite its wide occurrence in aquatic environments, polyP was mainly detected at top depth in lake and marine sediments, such as the top 0.5−2 cm of Effingham Inlet overlain by oxic waters and 22 European lakes based on solid-state ^{31}P nuclear magnetic resonance (NMR) spectroscopy analyses.[9,10] The lack of direct evidence for polyP presence in sediments at greater depth was possibly due to its rapid transformation after entering sediment environments. Indeed, polyP have been reported to readily undergo acid or base hydrolysis,[16−18] as well as rapid transformation into orthophosphate (orthoP) during diagenesis in sediments and in water columns.[10,15] The preferential recycling of polyP relative to total particulate phosphate (TPP) in seawater columns was likely linked to polyP hydrolysis catalyzed by alkaline phosphatase.[15,19] Yet, the roles of soil and sediment mineral components on the uptake and/or transformation of polyP still remain poorly understood.

A recent study showed that triphosphate (P_3) adsorbed on goethite can be fully hydrolyzed at pH 4.5 and slightly hydrolyzed at pH 6.5 and 8.5 within 3 months.[20] Our recent study showed that polyP can be hydrolyzed at the surface of γ-Al_2O_3 (an analogue of natural Al oxides), which was affected by mineral particle size and solution chemistry such as pH and the presence of metal cations.[21] Amorphous MnO_2 showed high reactivity toward P_3 hydrolysis (i.e., complete degradation into three orthoP molecules within 2 h at pH 4.0), and the hydrolysis rate in natural lake water was further promoted due to the presence of Ca^{2+} and Mg^{2+}.[22] Thus, mineral catalyzed hydrolysis is expected to play an important role in polyP transformation at environmental interfaces, yet related investigations are few.

Additionally, degradation of polyP can lead to local high concentrations of orthoP that can act as a potential source for the precipitation of Ca-phosphate minerals in the presence of Ca^{2+}. Our recent research on phosphatase-mediated hydrolysis of linear polyP revealed the fast release of orthoP into solution and the precipitation of amorphous Ca-phosphate solid(s) in the presence of Ca^{2+}.[19] Metal oxides (e.g., Mn, Fe, Al oxides) typically have high surface areas and large amounts of reactive surface sites that can facilitate processes such as adsorption or coadsorption of cations and anions, thereby creating micro-environments with concentrated ions that can potentially induce or facilitate surface precipitation.[23] For instance, coadsorption and complexation of Ca^{2+} and phosphate on boehmite (γ-AlOOH) surface facilitated the surface precipitation of hydroxylapatite at pH 7−9.[23]

In this study, we systematically investigated the rapid hydrolysis of polyP by Mn oxides with varied structures (α-MnO_2, β-MnO_2, δ-MnO_2, and birnessite), as well as the effects of polyP phase (dissolved vs solid) and structure (e.g., chain length), and type and concentration of common metal cations (Ca^{2+}, Mg^{2+}, Cu^{2+}, Zn^{2+}, and Mn^{2+}). The four MnO_2 are structurally distinct, and represent natural Mn oxide phases with dominating layer and tunnel structures.[24,25] δ-MnO_2 and birnessite are two layered phyllomanganate phases, both with hexagonal symmetry but with different structural order. Birnessite has better crystallinity, larger particle size, more layer stacking, and lower surface area as compared to δ-MnO_2.[25] α-MnO_2 (2 × 2 tunnels) and β-MnO_2 (pyrolusite, 1 × 1 tunnels) represent tunnel structured Mn oxides with varied tunnel size.[24,26] In this study, complementary batch experiments, solution ^{31}P NMR and X-ray absorption spectroscopy (XAS) analyses were conducted to reveal the evolution of solution and solid phases during polyP interaction with Mn oxides. Results from this study can provide new insights for the abiotic transformation of polyP at environmental interfaces, which will aid the advancement of our understanding on P cycling in aquatic environments.

EXPERIMENTAL SECTION

Materials and Characterization. Pyrophosphate and polyphosphates (with average chain length of 3−45) were used for the hydrolysis experiments. Sodium pyrophosphate tetrabasic decahydrate ($Na_4P_2O_7{\cdot}10H_2O$, hereafter P_2), sodium triphosphate pentabasic ($Na_5P_3O_{10}$, hereafter P_3), polyphosphate sodium salt (Na-polyP, hereafter P_{10}) and sodium phosphate glass (type 45, hereafter P_{45}) were purchased from Sigma-Aldrich. Sodium hexametaphosphate [$Na_6(PO_3)_6$, ring structure, hereafter P_6] was purchased from Alfa Aesar. All reagents were used as is. Information on the syntheses and characterization of calcium polyphosphate (Ca-polyP) granules, α-MnO_2, β-MnO_2, δ-MnO_2, birnessite and varied polyP are provided in the Supporting Information (SI) Text S1.

Mn Oxide Catalyzed Hydrolysis of Polyphosphates. Prior to the hydrolysis experiments, 0.04 g Mn oxides (α-MnO_2, β-MnO_2, δ-MnO_2, or birnessite) and 0.58 g NaCl (as background electrolyte, equivalent to 0.1 mM) were added to 98.75 mL DI water in a 125 mL wide-mouth glass bottle and stirred for 18 h. After overnight dispersion, pH values of the suspension were manually adjusted to 6.0 ± 0.05 using 0.05 M HCl or NaOH. Buffers were not used to avoid potential interaction with polyP and/or mineral surfaces. To initiate polyP hydrolysis reaction, 1.25 mL of polyP (P_{10}) stock solution (containing approximately 40 mM total phosphate) was added into the suspension, and the suspension pH was immediately adjusted to 6.0 using 0.05 M HCl or NaOH. During the reaction, pH of the suspensions was manually adjusted within the first 2 h, then at 3, 5, 7, 10, 24, 48, 72, and 96 h. At specific time points, 2 mL aliquots of the suspension were taken and immediately filtered through 0.22 μm Millipore membranes. The filtrate was analyzed for orthoP production and total P concentrations. OrthoP concentration was determined using the phosphomolybdate colorimetric assay[27] on an UV−vis spectrometer (Carey 60, Agilent). For total P measurement, all P in the supernatant was first hydrolyzed to orthoP using the potassium persulfate autoclave digestion method,[28] then analyzed using the phosphomolybdate colorimetric assay. All experiments were performed in duplicate.

Several parallel experiments were conducted to explore the effects of metal cation type and concentration, polyP chain length, and polyP phase (dissolved vs solid granules). (1) For experiments exploring Ca^{2+} effects, 1 mL stock solution of $CaCl_2$ (50 mM) was added into 97.75 mL DI water before the addition of varied Mn oxides and NaCl, and the final Ca^{2+} concentration in the reaction suspension was 500 μM; (2) For hydrolysis experiments of polyP with varied chain length and α-MnO_2 in the presence or absence of Ca^{2+}, 1.25 mL of P_2, P_3, P_6, or P_{45} stock solution (each containing total P concentration of 40 mM) was added into 98.75 (no Ca^{2+}) or 97.75 mL (with

DOI: 10.1021/acsearthspacechem.9b00220
ACS Earth Space Chem. 2019, 3, 2623−2634

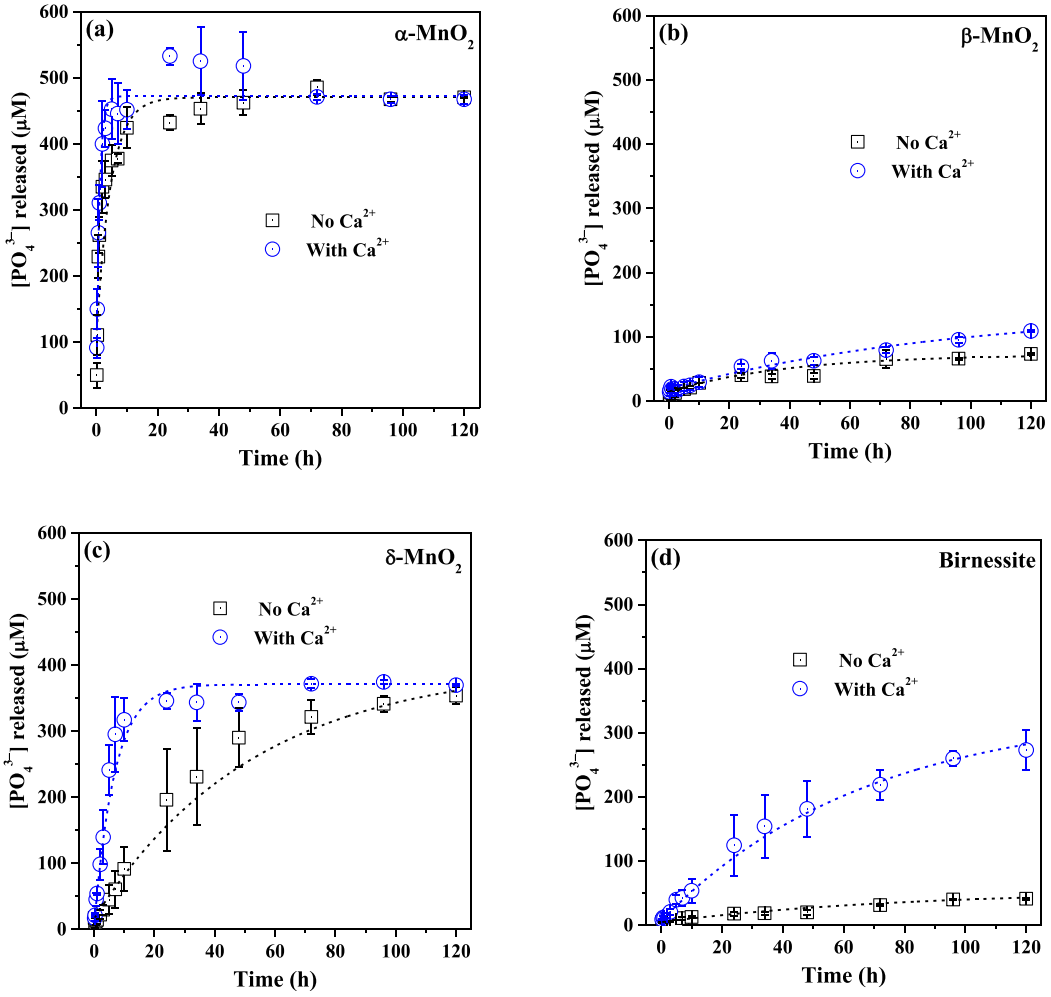

Figure 1. Phosphate release as a function of time during polyphosphate (P_{10}) reaction with α-MnO_2 (a), β-MnO_2 (b), δ-MnO_2 (c), and birnessite (d) at pH 6.0 with or without 500 μM Ca^{2+}.

500 μM Ca^{2+}) prepared α-MnO_2 suspension; (3) For hydrolysis experiments of Ca-polyP solid granules by α-MnO_2, 0.02 g of the synthesized Ca-polyP granules was added into 100 mL of 0.4 g L^{-1} α-MnO_2 suspension with 0.1 M NaCl electrolyte at pH 6.0, 7.5, or 9.0; (4) For hydrolysis of P_{10} by δ-MnO_2 with different Ca^{2+} concentrations or different metal cations (Ca^{2+}, Mg^{2+}, Cu^{2+}, Zn^{2+}, Mn^{2+}), calculated amount of the stock solution of the metal cations (chloride salts) was added into 97.75 mL deionized water to reach the desired final concentration (5, 10, 20, 50, 150, 500 μM for Ca^{2+}; 500 μM for Mg^{2+}, Cu^{2+}, Zn^{2+}, and Mn^{2+}), then 0.01 g δ-MnO_2 was added to prepare the dispersed suspension. During all experiments, concentrations of metal cations in the filtered supernatant were measured by inductively coupled plasma−mass spectroscopy (ICP-MS). In order to better isolate reaction processes such as surface adsorption and hydrolysis, our kinetic studies mainly focused on pH 6.0 (representative of fresh water environments), due to potential surface or solution precipitation of Ca^{2+} with polyP or orthoP (hydrolysis product) at high pH values. Relatively high concentration of metal cations (Cu^{2+}, Zn^{2+}, and Mn^{2+}) were used in order to clearly demonstrate their promotion effects on polyphosphate hydrolysis on the surface of Mn oxides and for consistency with Ca^{2+} and Mg^{2+} concentrations used. The effect of polyP phase (solid vs dissolved) on its hydrolysis was investigated at pH 6−9 (representing fresh water to seawater conditions).

NMR Analysis. In order to characterize the transformation of dissolved polyphosphates during mineral-catalyzed hydrolysis, parallel experiments were conducted for ^{31}P solution NMR characterization. Because total P concentration in the supernatant prepared in the Mn Oxide Catalyzed Hydrolysis of Polyphosphates section was not high enough, solution ^{31}P NMR spectra of the supernatant did not yield good signal-to-noise ratio. In order to obtain decent spectra within a reasonable time frame, the supernatant for NMR analysis was prepared at the same pH condition (6.0 ± 0.05) but by increasing the concentrations of polyP, Ca^{2+}, and Mn oxides by a factor of 6. At specific time points, 5 mL suspension was taken and immediately centrifuged and filtered through a 0.22-μm Millipore membrane, and the supernatant was used for solution ^{31}P NMR measurement. Solution ^{31}P NMR spectra were collected on a Bruker AMX 400 MHz spectrometer operated at 162 MHz and 297 K. A 90° pulse width, 6.5k data points (TD) over an acquisition time of 0.51 s, and relaxation delay of 15 s were applied. Chemical shift was calibrated using 85% H_3PO_4 as the external standard. At least 512 scans were collected for each spectrum (equivalent to ∼1 h).

P and Mn XAS Analysis. For hydrolysis experiments using the synthesized Ca-polyP solid granules (details in the

DOI: 10.1021/acsearthspacechem.9b00220
ACS Earth Space Chem. 2019, 3, 2623−2634

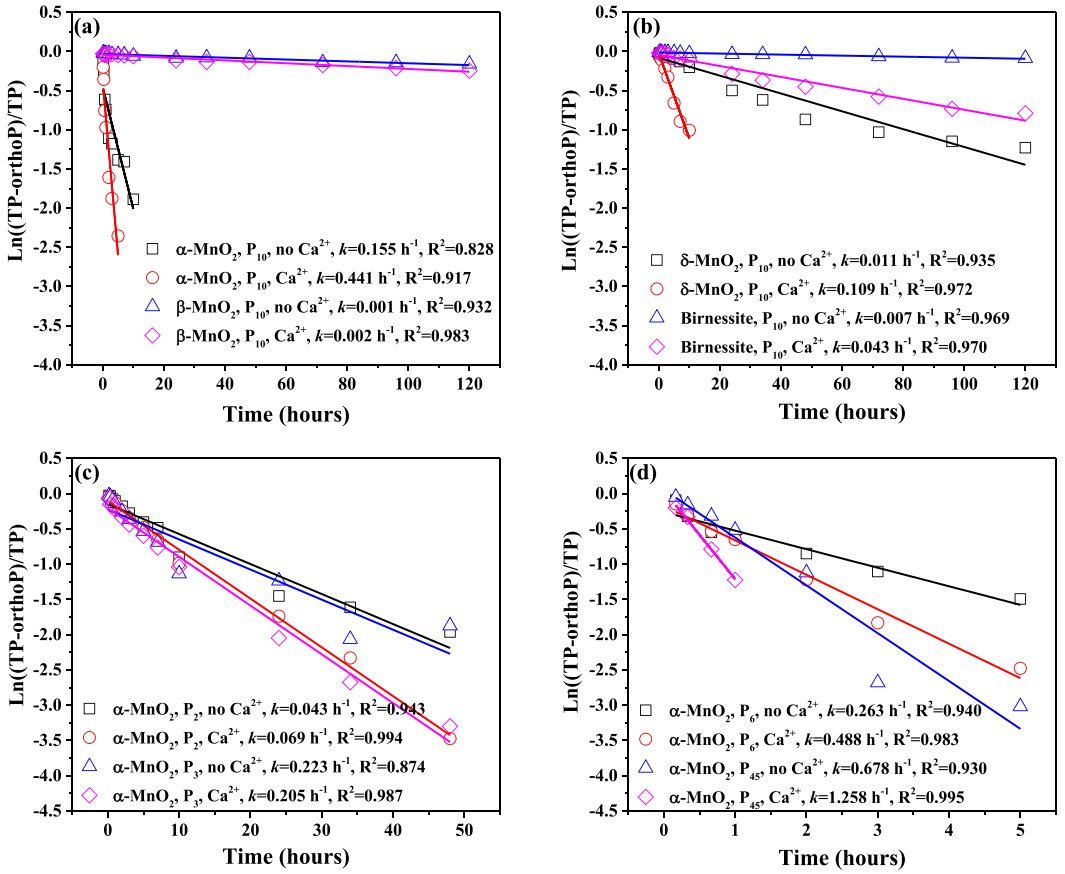

Figure 2. Hydrolysis of various polyphosphates by Mn oxides (0.4 g L^{-1}) at pH 6.0 with or without 500 μM Ca^{2+}. Solid lines present the first-order kinetic model fitting results of P_{10} hydrolysis on α- and β-MnO_2 (a), P_{10} hydrolysis on δ-MnO_2 and birnessite (b), P_2 and P_3 hydrolysis on α-MnO_2 (c), and P_6 and P_{45} hydrolysis on α-MnO_2 (d), in the presence or absence of 500 μM Ca^{2+}.

Materials and Characterization section), freeze-dried samples before and after reaction were analyzed by P K-edge X-ray absorption near edge structure (XANES) spectroscopy at Beamline 14−3 at the Stanford Synchrotron Radiation Lightsource (SSRL), Menlo Park, CA. Finely ground powders were brushed evenly onto P-free Kapton tape and mounted to a sample holder maintained under helium atmosphere. XANES data were collected in fluorescence mode using a PIPS detector. Energy calibration used $AlPO_4$ (edge position at 2152.8 eV). XANES spectra were collected at 2100−2485 eV. At least 2 scans were collected for each sample. Since Ca-polyP granules were used for studying the hydrolysis and precipitation, orthophosphate produced from the hydrolysis reaction can either adsorb onto α-MnO_2 or form Ca phosphate precipitates. Therefore, a suite of P reference compounds were prepared for XANES analysis: (1) polyphosphate sodium salt (Na-polyP) (Sigma-Aldrich) and synthesized Ca-polyP granules, representing solid polyphosphates; (2) orthophosphate sorbed on α-MnO_2 (details in SI Text S2), representing Mn oxide associated P; (3) amorphous calcium phosphate (ACP), octacalcium phosphate (octaCa), and hydroxyapatite,[29] representing calcium phosphate precipitates. XANES spectra of all reference compounds were collected in the same manner as for unknown samples. Data analysis used the software Ifeffit.[30] All spectra were carefully examined for energy calibration, merged, and normalized. Linear combination fitting (LCF) was conducted on the XANES spectra at energy range of 15−50 eV relative to the edge energy. The goodness of fit was evaluated using the residual factor (R-factor), and the fit with smallest R-factor was deemed the best fit. Mn K-edge XAS analysis was also conducted for the Mn oxides, with experimental and data analysis details in SI Text S3.

RESULTS AND DISCUSSION

Hydrolysis of Polyphosphate (P_{10}) by Mn Oxides and Effect of Mineral Structure. Mn oxides with varied structures showed different reactivity toward polyP hydrolysis. The effect of four Mn oxides (α-MnO_2, β-MnO_2, δ-MnO_2, and birnessite) toward P_{10} hydrolysis is shown in Figure 1. Orthophosphate was produced and released to the solution during P_{10} hydrolysis, and its production kinetics can be fitted by first-order kinetic model (Figures 2a,b and Table S1). The degradation of polyP is a very complicated kinetic process involving the one-by-one hydrolysis of the terminal phosphate groups (the mechanism explained below) and the gradual shortening of the polyP chain length. First-order kinetic model showed the best fitting results when compared with zeroth-order and second-order fitting results. α-MnO_2 showed the highest rate and extent toward polyP hydrolysis and was able to hydrolyze all P_{10} within 10 h (Figure 1a). This is consistent with the results from a previous study that α-MnO_2 showed higher rate of hydrolysis for *p*-nitrophenyl phosphate than other Mn oxides.[31] The hydrolysis rate roughly followed the order of α-MnO_2 > δ-MnO_2 > birnessite > β-MnO_2, regardless of Ca^{2+} presence (Table S1 and Figures 2a,b). The higher hydrolysis rates of α-MnO_2 and δ-MnO_2 can be related to their higher surface areas; both are ~70 times of β-MnO_2 and ~5 times of birnessite. In the control experiment, only

DOI: 10.1021/acsearthspacechem.9b00220
ACS Earth Space Chem. 2019, 3, 2623−2634

2.8% of polyP was degraded after 5 d experiment in 500 μM Ca^{2+} solution without the existence of MnO_2. The presence of 500 μM Ca^{2+} enhanced the hydrolysis rates for all four Mn oxides, especially for δ-MnO_2 and birnessite (Table S1 and Figures 2a,b). For example, in the presence of 500 μM Ca^{2+}, α- and δ-MnO_2 were able to hydrolyze all P_{10} within 5 and 24 h, respectively.

The change of total P concentration in solution was used to evaluate the sorption/uptake of both polyP and orthoP (released from hydrolysis) onto mineral surfaces (Figure S4). The evolution of total P concentration in solution during mineral-catalyzed hydrolysis differed from the adsorption of orthoP or organic phosphate on metal oxides, where dissolved P concentration typically continuously decreases with the increase of reaction time.[32] For our polyP-mineral hydrolysis system, in general, solution total P increased drastically during the first few hours of reaction, followed by a steady state, suggesting polyP interface behavior to be an adsorption-hydrolysis process. At the initial stage, polyP rapidly adsorbed onto Mn oxides. As the reaction proceeded, the hydrolysis of polyP and release of orthoP led to the increase of total P concentration in the supernatant. From the change of total P concentration in solution, δ-MnO_2 showed a higher affinity for both polyP and orthoP species and adsorbed a relatively larger amount of polyP and orthoP at the surface than other Mn oxides (Figure S4). Figure S5a showed that δ-MnO_2 has the highest content of surface adsorbed Ca^{2+}. Adsorbed Ca^{2+} can likely promote polyP and orthoP adsorption by compensating negative mineral surface charge, increasing the electrostatic attraction of polyP and orthoP toward the mineral surface, and potentially promoting the formation of ternary surface complexes.[22,23,33] Such higher coverage of polyP due to Ca^{2+} presence likely resulted in the enhanced hydrolysis of polyP by Mn oxides, as discussed later.

Solution ^{31}P NMR spectroscopy revealed the alteration of P speciation in the filtrate after 5-day hydrolysis of polyP by Mn oxides (Figure 3). For δ-MnO_2 and birnessite systems, the presence of 500 μM Ca^{2+} remarkably increased the intensity of NMR signal for orthoP at 0.43 ppm, and decreased the NMR signal for polyP at −8 and −22 ppm (Figures 3c,d) (for polyP terminal and middle phosphate groups, respectively).[19] Such enhancement is consistent with batch experiment results that the presence of Ca^{2+} significantly enhanced polyP hydrolysis by δ-MnO_2 and birnessite, but had minimal effects on α-MnO_2 system (which already had the highest hydrolysis rate). For example, δ-MnO_2 hydrolyzed most of polyP over 5 d; when Ca^{2+} was added, no residual polyP was detected in the filtrate by NMR. In the α-MnO_2 system, only a single NMR peak at 0.43 ppm was observed, suggesting that no polyP remained after 5-d reaction even without Ca^{2+} addition, consistent with the result of batch experiments (Figures 1a, 3a). The difference of intensity for the orthoP peak in Figure 3a is due to the difference in numbers of scans (2048 scans for experiments without Ca^{2+}, 512 scans for experiment with Ca^{2+}). Overall, the NMR results further confirmed that the reactivity of Mn oxides toward polyP hydrolysis was in the order of α-MnO_2 > δ-MnO_2 > birnessite > β-MnO_2.

Effect of Polyphosphate Chain Length. Previous studies have revealed a terminal-only hydrolysis pathway of polyP by proton[17] and enzymes.[19] Our recent study demonstrated that polyP molecules with longer chain length had lower hydrolysis rate and extent during their interaction with phosphatase enzymes, due to higher molecular concentration of the shorter

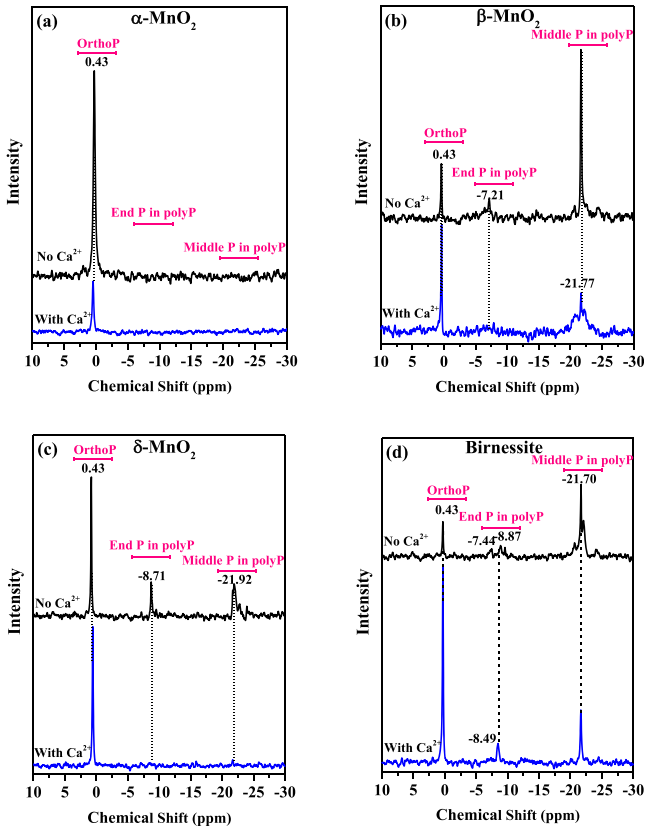

Figure 3. ^{31}P solution NMR spectra of liquid supernatants obtained after polyphosphate (P_{10}) reaction with α-MnO_2 (a), β-MnO_2 (b), δ-MnO_2 (c), and birnessite (d) at pH 6.0 with or without 500 μM Ca^{2+} for 5 d.

chained polyphosphates at the same total P concentration.[19] Here, the hydrolysis of polyP with varied chain length by α-MnO_2 was compared, where all polyP experiments started with the same total P concentration. The hydrolysis rate of longer chained polyP (P_6, P_{10}, and P_{45}) was relatively higher than that of short chained polyP (P_2 and P_3) (Figures 1a,2,4 and rate data summarized in Table S1). The hydrolysis rate of P_{45} was the highest, and the reaction completed within 3 h in the absence of Ca^{2+} and within 2 h in the presence of 500 μM Ca^{2+} (Figures 2d, 4, and Table S1). Complete hydrolysis of P_6 and P_{10} was achieved within ∼5 h in the absence of Ca^{2+} (Figures 1a, 4c). The hydrolysis of P_2 and P_3 was relatively slow, taking 36 h (P_2) and 24 h (P_3) until complete hydrolysis (Figures 4a,b). The presence of 500 μM Ca^{2+} enhanced both the hydrolysis rate and extent of α-MnO_2 toward all five polyP species, consistent with previous results that the presence of Ca^{2+} enhanced the hydrolysis rate of triphosphate by MnO_2 in Lake Northam water.[22] The supernatant P concentration during longer chained polyP reaction with α-MnO_2 at the first time point (10 min) was lower than that of shorter chained polyP (Figure S6). These results may result from more phosphate groups of long chain polyP per molecule and Mn oxide mineral being able to fix much more total P for longer chained polyP adsorption in comparison with shorter chained species. The presence and adsorption of Ca^{2+} can also decrease total P concentration of five polyP species in the supernatant at initial reaction stage (Figure S6).

A series of supernatants at different reaction times were selected to perform time-resolved solution ^{31}P NMR measure-

DOI: 10.1021/acsearthspacechem.9b00220
ACS Earth Space Chem. 2019, 3, 2623−2634

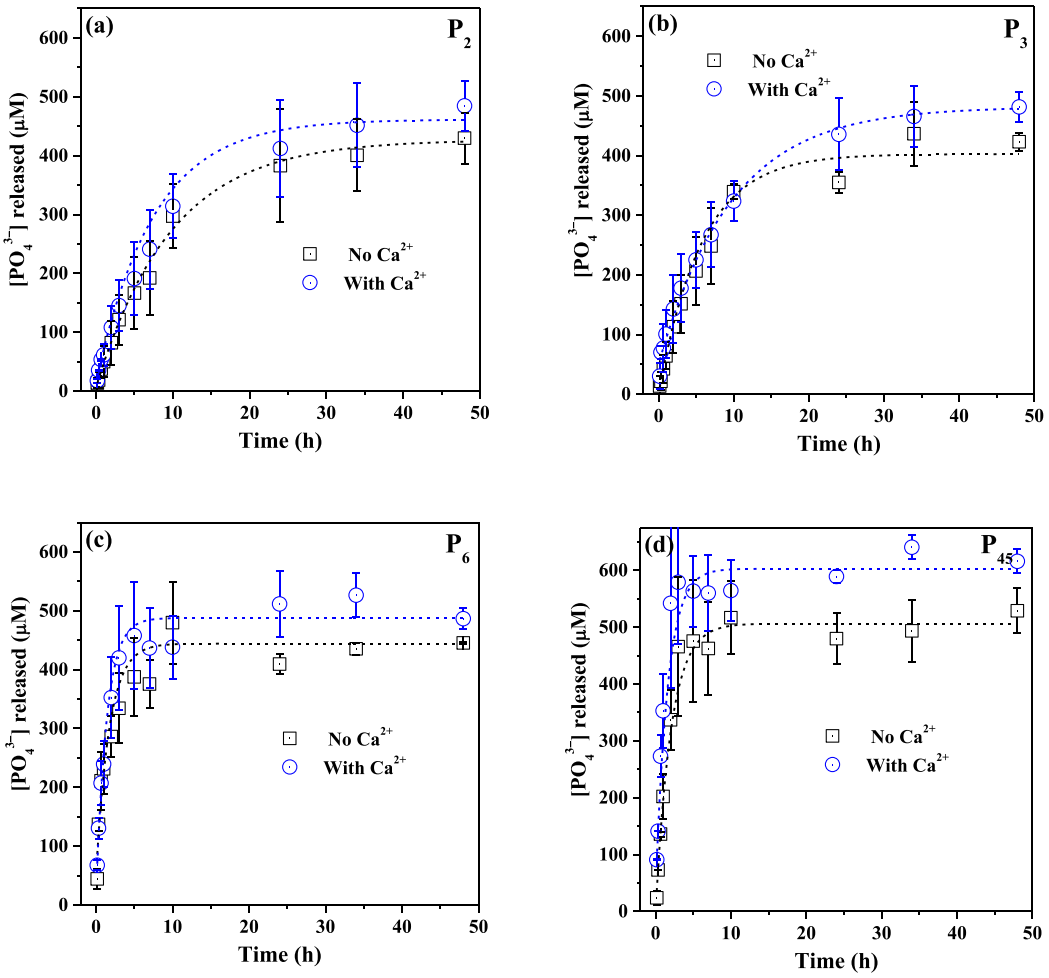

Figure 4. Phosphate release as a function of time during the interaction of α-MnO_2 with polyphosphates with varied chain lengths: (a) P_2, (b) P_3, (c) P_6, and (d) P_{45}. Experiments were conducted at pH 6.0 with or without 500 μM Ca^{2+}.

ments (Figure 5) to reveal the evolution of P speciation during the hydrolysis of five polyP species by α-MnO_2. The NMR results indicated that the hydrolysis rates of longer chained polyP were higher than those of shorter chained ones, consistent with the results from batch experiments. The NMR signals of longer chained polyP completely disappeared within 1 h (Figures 5c–e). This period was shorter than that in batch experiments, likely due to the differences in polyP and Mn oxide concentrations used. A closer examination of the NMR spectrum of P_{10} hydrolysis by α-MnO_2 after 10 min of reaction showed the coexistence of signals for orthoP and polyP (Figure S7). During the degradation of long chained polyP, their time-resolved NMR spectra did not show the chemical signals of shorter chained polyP (Figures 5c–e). In combination with the rapid and continuous orthoP release in batch experiments, we propose that mineral-catalyzed hydrolysis of polyP also proceeds with the terminal-only hydrolysis mechanism, similar to enzymatic hydrolysis of polyP.[19]

After 24 h reaction, some P_2 and P_3 signals still remained for the hydrolysis of P_2 and P_3 (short chain polyP), respectively (Figures 5a,b). The slow disappearance of P_2 or P_3 NMR signals in their reacted supernatant implied slow hydrolysis rates of these two polyPs over 24-h reaction times. In time-resolved NMR spectra of P_3 hydrolysis, the intensity of the peaks at around −7.5 and −22.3 ppm rapidly decreased and the peak at −9.15 ppm (belonging to P_2) gradually increased and persisted even after 24 h reaction (Figure 5b). At 0.5 h, the peak at around −9.69 ppm showed a broad shoulder, which contained overlapping signals from both P_2 and P_3 end groups, possibly due to the close chemical shift of P_2 and P_3's terminal P groups or the potential magnetic interference from very fine α-MnO_2 particles that might have passed through the 0.2-μm syringe filter.

In order to explore the effect of Ca^{2+} and obtain better signals, we conducted a separate set of NMR experiment by reducing the concentration of α-MnO_2 by 6-fold and adding 3 mM Ca^{2+}, and the results are shown in Figure S8. With the lower concentration of α-MnO_2, the reaction time needed for complete hydrolysis of P_3 increased to 96 h. For this experimental set, time-resolved NMR spectra showed that the concentration of P_2 first increased then decreased as the reaction proceeded, and orthoP was continuously produced as the degradation product of P_3 and P_2. Our NMR results are consistent with a previous study using anion exchange chromatography to identify the hydrolysis products of P_3 in Lake Northam water in the presence of amorphous MnO_2 (Figure S8).[22] The hydrolysis pathway of P_3 thus is consistent with the above-mentioned terminal-only hydrolysis mechanism, i.e., through the degradation of one P_3 molecule to produce one P_2 and one orthoP, followed by the degradation of the produced P_2 to two orthoP molecules.

DOI: 10.1021/acsearthspacechem.9b00220
ACS Earth Space Chem. 2019, 3, 2623–2634

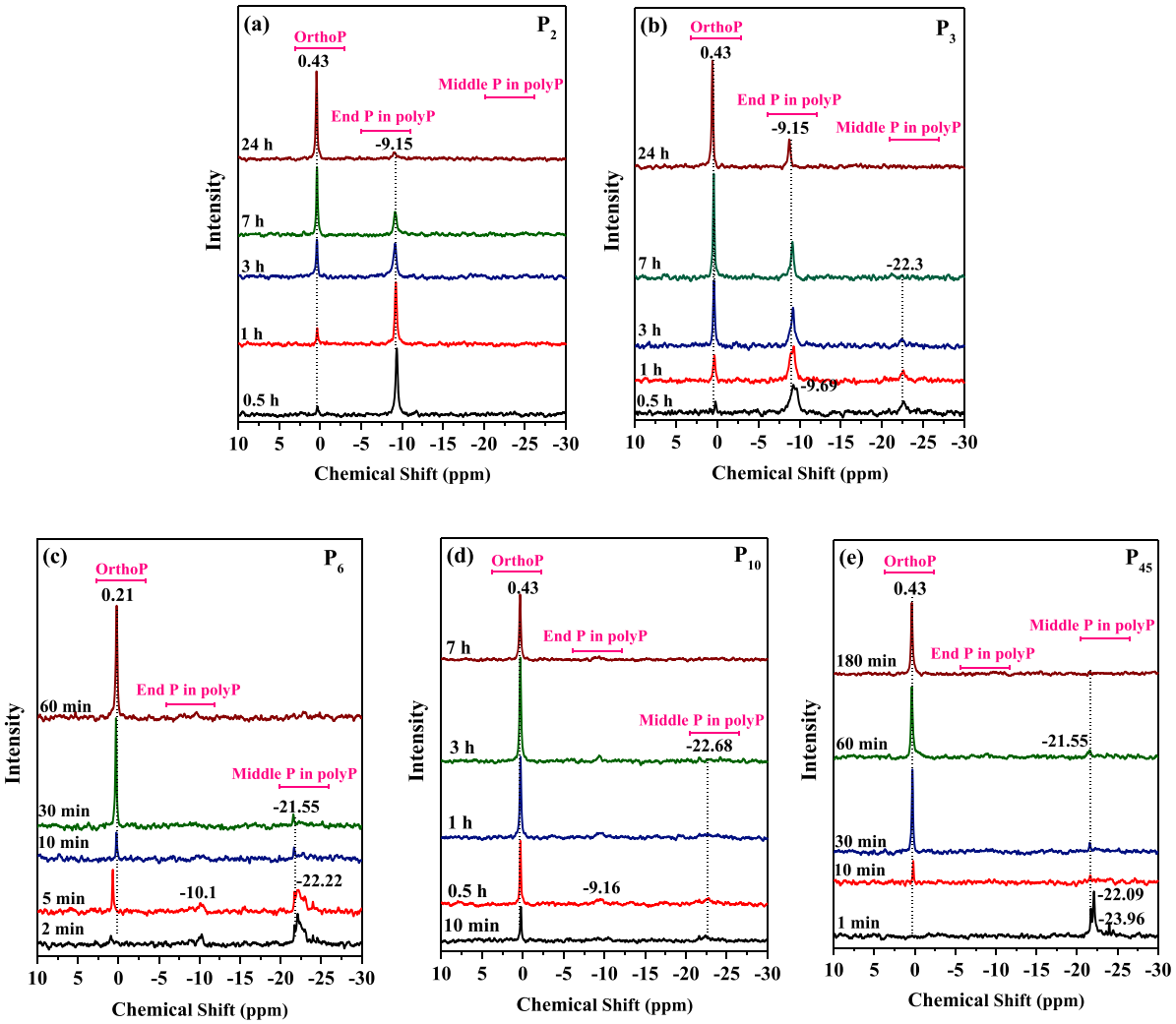

Figure 5. Time-resolved ^{31}P solution NMR spectra of liquid supernatant after the reaction of polyphosphates of varied chain length with α-MnO_2 without Ca^{2+} addition at pH 6.0. Panels (a–e) are for P_2, P_3, P_6, P_{10}, and P_{45}, respectively.

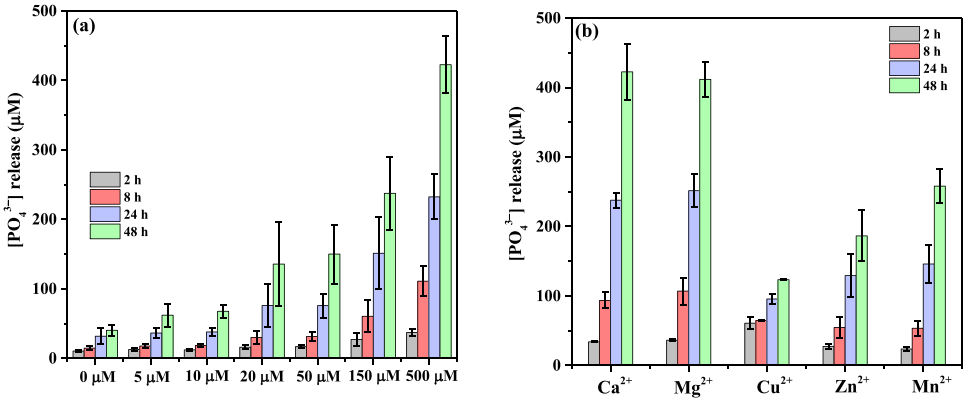

Figure 6. Effect of (a) varied Ca^{2+} concentration (0–500 μM) and (b) different metal cations at 500 μM on surface-catalyzed hydrolysis of polyphosphate (P_{10}) by δ-MnO_2 at pH 6.0.

Effect of Metal Cations. The promotion of Ca^{2+} on the hydrolysis process prompted us to further investigate the effects of varied Ca^{2+} concentration and other divalent metal cations on the hydrolysis of polyP by Mn oxides (Figure 6). For this set of experiments, δ-MnO_2 was used and at a lower concentration of 0.1 g L^{-1} (compared to 0.4 g L^{-1} used for previous experiments), because α-MnO_2 or high concentration of δ-MnO_2 can lead to rapid degradation of polyP even without the presence of metal cations, making it difficult to differentiate the effect of Ca^{2+} and other divalent metal cations. Figure 6a showed that increasing the concentration of Ca^{2+} increased the extent of polyP hydrolysis. In the presence of 500

DOI: 10.1021/acsearthspacechem.9b00220
ACS Earth Space Chem. 2019, 3, 2623–2634

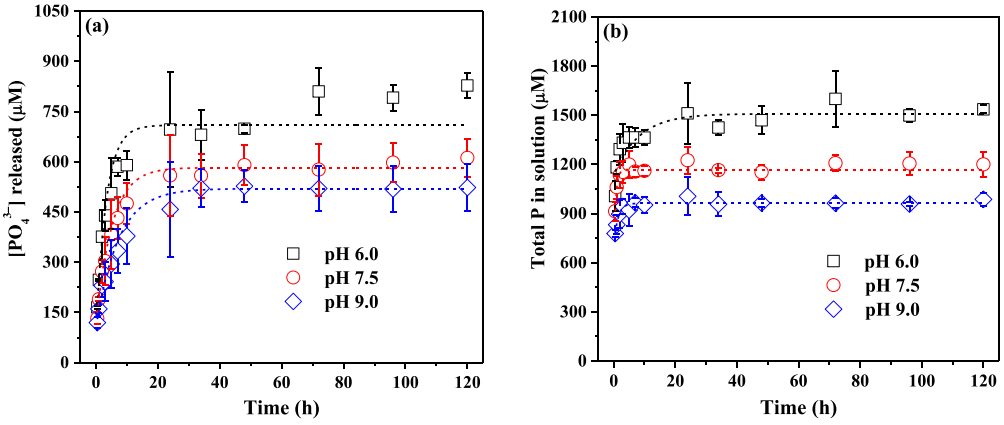

Figure 7. Change of phosphate (a) and total phosphorus concentration (b) as a function of time during the hydrolysis of calcium polyphosphate granules catalyzed by α-MnO_2 at pH 6.0, 7.5, and 9.0.

μM Ca^{2+}, δ-MnO_2 hydrolyzed all polyP to orthoP within 48 h, while in the absence of Ca^{2+} only 8% polyP was hydrolyzed (Figure 6a). Dissolved total P concentration showed no obvious difference at different reaction times and/or Ca^{2+} concentrations (Figure S9a). This is likely due to the low concentration of δ-MnO_2 (0.1 g L^{-1}) and high concentration of total P (500 μM) in the suspension. The low surface coverage of P on δ-MnO_2 (~260 μM orthoP per g δ-MnO_2, Figure S10) can hardly change the total P concentration in solution. Figure S9b showed Ca^{2+} uptake by δ-MnO_2. At high Ca^{2+} loadings, there was still much Ca^{2+} remaining in solution. For example, at Ca^{2+} concentration below 10 μM, almost all Ca^{2+} was adsorbed onto the surface of δ-MnO_2; when Ca^{2+} was added to 500 μM, approximately 350 μM Ca^{2+} stayed in solution. The presence of surface adsorbed and/or free dissolved Ca^{2+} may enhance the formation of mineral-Ca-polyP ternary surface complex and/or Ca-polyP solution complexes. Figure 6b compared the effects of five common divalent metal cations (Ca^{2+}, Mg^{2+}, Cu^{2+}, Zn^{2+}, and Mn^{2+}) on the hydrolysis of polyP by δ-MnO_2. In general, all metal cations showed enhanced hydrolysis extent as compared to no-divalent metal controls (Figure 6a). At the same metal cation concentration, orthoP release from polyP hydrolysis followed the order of $Ca^{2+} \geq Mg^{2+} > Mn^{2+} > Zn^{2+} > Cu^{2+}$ (Figure 6b). Figure S9d showed a higher amount of $Cu^{2+}/Zn^{2+}/Mn^{2+}$ uptake by δ-MnO_2 surface. Total P uptake by δ-MnO_2 in the presence of Cu^{2+}, Zn^{2+}, and Mn^{2+} was also higher than that in the presence of Ca^{2+} and Mg^{2+} (Figure S9c), possibly due to the stronger affinity of $Cu^{2+}/Zn^{2+}/Mn^{2+}$ to phosphate groups and Mn oxide surface.[34,35]

Hydrolysis of Ca-PolyP Solid Granules. The effect of polyP phase (solid vs dissolved) on its hydrolysis was also investigated in the presence of α-MnO_2 (Figure 7), as previous studies have suggested the abundant presence of scattered micron-sized Ca-polyP particles in marine sediments.[12] The choice of α-MnO_2 was based on the fastest hydrolysis rate of polyP by α-MnO_2, which may make it easier to observe solid Ca-polyP transformation. The concentration of both total P and produced orthoP in solution increased as the reaction proceeded and reached steady state at around 24 h at pH 6.0, 7.5, and 9.0 (Figure 7). At steady state, the total P concentration in solution was ~1.7 times of orthoP concentration. The increase of total P concentration resulted from the rapid and continuous dissolution of Ca-polyP solid granules. The resulting dissolved polyP could be adsorbed onto α-MnO_2 followed by hydrolysis and production of orthoP. Thus, at the initial stage, the concentration of total P was very high with minor amount of orthoP in the supernatant, and a ratio of total P to orthoP in the supernatant was around 10 (Figure 7). Meanwhile, pH had obvious impacts on the concentrations of orthoP and total P in solution. The concentrations for both orthoP and total P were significantly higher at pH 6.0 than at pH 9.0 and pH 7.5, suggesting that the dissolution of Ca-polyP granules was dominated by proton-promoted mechanism. However, the larger amount of orthoP release at pH 6.0 can not be solely correlated to proton hydrolysis of polyP, as at this pH the concentrations of total P and Ca^{2+} (Figure S5c) were also higher than those at pH 9.0.

Because total P concentration in the solution is higher than orthoP concentration, the solution should also contain unreacted polyP from the dissolution of Ca-polyP granules. Therefore, solution ^{31}P NMR analysis was conducted to investigate the change of P speciation in the supernatant (Figure S11). When pH increased from 6.0 to 9.0, the signals of orthoP and polyP end groups shifted from 0.56 to 2.39 ppm for orthoP and from −7.66 to −5.77 ppm for polyP end phosphate group. At 1 h reaction time, the signals for polyP were at around −7 and −22 ppm and the peak intensities were higher at pH 9.0 (compared to pH 6.0). ^{31}P solution NMR spectra revealed the presence of large amounts of orthoP in solution at all three pH values, consistent with the rapid dissolution of Ca-polyP granules and hydrolysis of released polyP. The gradual increase of the intensity of polyP signals with increasing pH suggests the faster dissolution of Ca-polyP granules and/or slower hydrolysis of released polyP at lower pH. This is consistent with the result from batch experiments. After 5-d reaction, signals for polyP were very weak and hard to detect by NMR in all samples, likely due to the low concentration of total polyP molecules (10 PO_4 units per polyP molecule). Consistent with this, the NMR signal for orthoP dominated the whole spectra. These results indicated that only a small amount of polyP remained in the solution and the ratio of polyP to orthoP decreased significantly (in batch experiment, decreased from ~10 to ~1.7) after 5-day reaction. The results from both batch experiments and NMR spectroscopy suggest the rapid transformation of solid Ca-polyP into dissolved polyP and eventually dissolved orthoP.

Previous studies reported that the total dissolved Ca^{2+} and P concentrations required for supersaturation with respect to Ca-polyP glass was more than 3 orders of magnitude higher than

DOI: 10.1021/acsearthspacechem.9b00220
ACS Earth Space Chem. 2019, 3, 2623−2634

those with respect to hydroxyapatite.[36] Due to the concurrent production of Ca^{2+} (from Ca-polyP dissolution) and orthoP (from the hydrolysis of polyP from Ca-polyP dissolution), the formation of new Ca-phosphate phase(s) is highly likely, especially at high pH values. P K-edge XANES spectroscopy was thus performed to reveal the structural and mineralogical information on the solid products after 5-day reaction (Figure 8b) and compared to a suite of reference compounds (Figure 8a). As can be seen from Figure 8a, Ca phosphate minerals exhibited a strong shoulder centered at ~2155 eV. For Ca phosphate minerals, highly crystalline compounds (such as octacalcium phosphate and hydroxylapatite) showed a second peak at ~2164 eV, and lower crystallinity phases such as amorphous calcium phosphate (ACP) exhibited less distinct shoulder peaks (Figure 8a), consistent with the spectra of previous P XANES standards.[37] The P XANES spectra of the solids after 5-day reaction did not show well separated shoulder peaks at ~2164 eV, implying that high crystallinity calcium phosphate mineral phases did not contribute a significant fraction (Figure 8b). Linear combination fitting (LCF) of the XANES spectra indicated the absence of crystalline calcium phosphate phases in the solid products (Table S2). With increasing solution pH, the relative percentage of ACP in the reacted solids increased from 59.4 ± 5.2% at pH 6.0 to 77.4 ± 3.6% at pH 9.0. Together with batch experiments and NMR results, LCF of P XANES suggested the overall transformation of Ca-polyP granules into amorphous calcium phosphate solids in the presence of α-MnO_2, and such transformation of solid phase was faster under alkaline pH conditions.

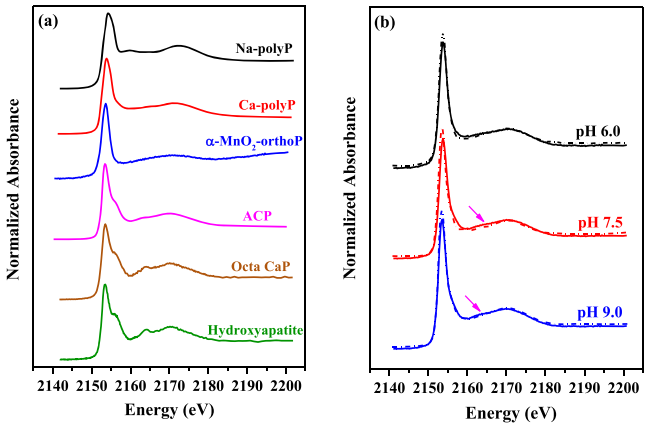

Figure 8. (a) P K-edge XANES spectra of phosphate reference compounds, including sodium polyphosphate salt (Na-polyP), synthesized calcium polyphosphate granules (Ca-polyP), α-MnO_2 adsorbed orthophosphate (α-MnO_2-orthoP), amorphous calcium phosphate (ACP), octacalcium phosphate (octaCaP), and hydroxyapatite. (b) Linear combination fitting of P XANES spectra of the solid reaction products from the hydrolysis experiments of Ca-polyP with α-MnO_2 at pH 6–9. Reaction condition: α-MnO_2 = 0.4 g L^{-1}; Ca-polyP granule = 0.02 g L^{-1}; NaCl = 0.1 M. Raw and fitted data are shown in dotted and solid lines, respectively. Fitting results are presented in Table S2.

Mechanisms of PolyP Hydrolysis on Mn Oxides. Due to the technical difficulties associated with obtaining/resolving spectroscopic signals, such as the magnetic property of Mn (difficult to collect solid NMR spectra), low surface coverage of phosphate sorbed on MnO_2 (hard to achieve good signal-to-noise ratio), and band overlap of phosphate vibration with MnO_2 mineral in IR spectroscopy, direct spectroscopic evidence for the formation of surface inner-sphere complexes is still lacking. However, formation of surface inner-sphere complexes was generally considered to be the main mechanism for phosphate adsorption on Mn oxides.[38] For example, a considerable decrease of Mn oxide point of zero charge (PZC) upon phosphate adsorption suggested formation of inner-sphere phosphate complexes.[39] Using pair distribution function (PDF) analysis of X-ray total scattering, the PDF spectra of phosphate adsorbed on birnessite indicated that the peaks at ~1.54 Å can be ascribed to the P–O pairs in the PO_4 tetrahedron and the peaks at ~3.14 Å are most likely due to P–Mn pairs,[40] also suggesting the formation of inner-sphere complexes on birnessite. Our recent solid state ^{31}P NMR results showed that, upon polyphosphate adsorption at the surface of γ-Al_2O_3, the main surface P species are phosphate groups in polyphosphate that formed direct bonds with the mineral surface as inner-sphere complexes (likely as bidentate binuclear complexes) and phosphate groups in polyphosphate that were not directly bonded to the mineral surfaces.[21] Due to similarity in P K-edge XANES spectra between α-MnO_2 adsorbed orthophosphate (α-MnO_2–orthoP) (Figure 8a) and Fe/Al oxide-adsorbed orthophosphate samples,[21,41] surface inner-sphere phosphate complexes are possible to form upon phosphate adsorption onto Mn oxides.

During polyphosphate hydrolysis, PO_4 groups were activated via the protonation of the double-bond oxygen to form 5-fold coordination intermediate, followed by a nucleophilic attack by water or hydroxyl molecules at acid pHs, or via direct attack by free hydroxyl ions at alkaline pHs.[17,18] During phosphate monoester hydrolysis by acid or alkaline phosphatase, an intermediate species was formed involving the oxygen atom of the terminal PO_4 group completely coordinated with two metal cations [e.g., Zn(II), Ca(II), Fe(II), Mn(II)].[42−44] These metal complexes in phosphatase can initiate double Lewis acid activation for hydrolyzing phosphates by initially bridging the two metal centers with the two phosphoryl oxygen atoms.[45] Based on the above-mentioned mechanisms for phosphate ester or polyP hydrolysis by proton, hydroxyl, and phosphatases, we propose that Mn oxide-catalyzed polyP hydrolysis probably derives from the ability of Mn atoms to coordinate with phosphate groups via oxygen atoms (either bidentate or monodentate configuration), which can activate the P atom for a nucleophilic attack. Surface H_2O and ≡Mn—OH groups are formed at Lewis acid Mn sites of Mn oxides (e.g., α-MnO_2 and δ-MnO_2), which are close to the neighboring Mn atoms coordinated with phosphoryl O atom,[46,47] and serve as a nucleophilic agent attacking the P atom with a subsequent cleavage of the P–O–P bond. Surface Lewis acid sites were previously confirmed as reactive centers for α-MnO_2 catalytic ozonation and Fe/Ce (hydro)oxide catalytic dephosphorylation.[46,48,49]

In comparison with polyphosphate hydrolysis on γ-Al_2O_3, Mn oxides showed several orders of magnitude higher activity than Fe/Al oxides.[21] The main difference between Mn and Al oxides is that Mn oxides have a high vacancy content in their structure.[50−52] The presence of vacancy sites at the surface of Mn oxides may be served as alternative active sites for dephosphorylation. Mn K-edge XANES of α-MnO_2 indicated the existence of ~10% Mn(III) in the structure of α-MnO_2 (Figure S12). Our recent study also reported 15% and 6% Mn(III) in δ-MnO_2 and birnessite, respectively.[25] The presence of structural Mn(III) or vacancy sites may result in

DOI: 10.1021/acsearthspacechem.9b00220
ACS Earth Space Chem. 2019, 3, 2623–2634

the decreased stability of P−O−P bonds of terminal phosphate groups that are readily attacked by hydroxyl groups adsorbed on nearby sites or free reactive hydroxyl groups. The direct quantitative relationship between polyP hydrolysis and vacancy site density is beyond the scope of this study and warrants future studies.

Key Factors Influencing PolyP Hydrolysis on Mn Oxides. Ca^{2+} can coordinate with the surface hydroxyl groups (≡Mn—OH) of Mn oxides, compensating the negative surface charge of Mn oxides,[53] thus enhancing the adsorption of negatively charged species such as polyP.[22] Ca^{2+} may also possibly form strong bonds with phosphate groups to form surface ternary complexes and serve as a cation bridge.[34] Due to the larger ionic radius of Ca atom (1.14 Å) compared to Mn (0.67 Å), we consider the formation of monodentate Ca-surface complexes to be more likely (as opposed to bidentate Ca surface complexes). Similar ternary surface complexes might also form in the presence of other divalent cations such as Zn^{2+}, Cu^{2+}, and Mn^{2+}, which can explain the enhanced hydrolysis of polyP in the presence of these cations. Compared to Mg^{2+} and Ca^{2+}, the relatively lower promotion effect of Zn^{2+}, Cu^{2+}, and Mn^{2+} on polyP hydrolysis may be attributed to the different adsorption mechanisms/sites of Zn^{2+}, Cu^{2+}, and Mn^{2+} on Mn oxides,[25,54,55] which might have affected the hydrolysis of polyP.

Comparing the hydrolysis efficiency of the four Mn oxides, it is clear that mineral structure, reactive site density, crystallinity, and surface properties (e.g., surface area) had distinct impacts on mineral-catalyzed polyP hydrolysis. For example, the hydrolysis rates of all four Mn oxides followed the order of α-MnO_2 > δ-MnO_2 > birnessite > β-MnO_2 (Table S1), which is consistent with their order of BET surface area: α-MnO_2 (146.43 ± 0.32 m^2 g^{-1}) > δ-MnO_2 (125.72 ± 0.6 m^2 g^{-1}) > birnessite (27.4 ± 0.6 m^2 g^{-1}) > β-MnO_2 (2.03 ± 0.07 m^2 g^{-1}). Comparing the hydrolysis of P_{10} by δ-MnO_2 and birnessite (which has similar crystal structure but different degrees of structure order), the less ordered and poorly crystalline δ-MnO_2 showed a higher hydrolysis rate as compared to the better ordered/crystalline birnessite. Due to the differences in crystallinity, δ-MnO_2 has higher surface area and higher site density of structural defects.[25] PolyP hydrolysis rates on α-MnO_2 (BET surface area: 146.43 ± 0.32 m^2 g^{-1}) and δ-MnO_2 (BET surface area: 125.72 ± 0.6 m^2 g^{-1}) are 0.155 and 0.011 h^{-1}, respectively, when no Ca^{2+} was added. α-MnO_2 presented a much higher hydrolysis rate for polyP hydrolysis than δ-MnO_2. The highest reactivity of α-MnO_2 for polyP hydrolysis may have also resulted from its reactive facets that may have more Lewis acid sites and higher vacancy content at the surface. High reactive facets and surface Lewis acid sites were previously confirmed as reactive centers for α-MnO_2 catalytic ozonation and arsenite oxidation.[46,56] For example, the (100) face of α-MnO_2 can form more stable surface complexes with arsenate and arsenite than the (110) face, and the (100) face is more functional for the removal of arsenate and arsenite than the (110) face.[56]

The terminal-only hydrolysis mechanism can explain the higher hydrolysis rate of long chained polyP, due to the stronger ability of long chained polyP molecules to compete with the released orthoP and/or short chained polyP molecules for adsorption onto Mn oxides. Additionally, only one terminal phosphate group of P_2 and P_3 could coordinate with the surface of Mn oxides, but another terminal phosphate group of longer chained poly P (P_6, P_{10}, and P_{45}) might be able to form bonds with the mineral surface, likely accompanied by some degrees of spatial constraints. For the hydrolysis of solid Ca-polyP granules, due to the release of Ca^{2+} and aqueous polyP from the dissolution of Ca-polyP granules, Ca^{2+} not only rapidly promoted the hydrolysis of aqueous polyP by α-MnO_2, but also served as a complexing cation with the orthoP produced from the hydrolysis of aqueous polyP, eventually leading to the precipitation of calcium phosphate solid(s), which might be an important pathway for P burial in marine sediments.

CONCLUSION

This study revealed the rapid hydrolysis and transformation (within hours or days) of polyP at the Mn oxide-water interface with the hydrolysis rate in the order of α-MnO_2 > δ-MnO_2 > birnessite > β-MnO_2. The presence of common divalent metal cations (Ca^{2+} and Mg^{2+}) can significantly enhance the hydrolysis of polyP by Mn oxides. The presence of other common metal cations (Cu^{2+}, Zn^{2+}, and Mn^{2+}) also has positive impacts on polyP hydrolysis by δ-MnO_2. Although the concentration of metals in our experiments is slightly higher than their environment concentrations, our results can be inferred for some natural systems. For example, microbial Mn/Fe reduction in soils and sediments may lead to high metal (e.g., Cu, Zn, and Mn) concentrations in the pore-water.[57,58] Calcium polyphosphate granules can be hydrolyzed by α-MnO_2, leading to the formation of amorphous calcium phosphate solid(s), which are often considered as precursors for apatite mineralization. The hydrolysis rates for longer chained polyP were relatively higher than those of shorter chained ones. PolyP with shorter chain lengths showed relatively slower hydrolysis rates, which might help explain the presence of high fractions of pyrophosphate in natural sediments and soils.[59] These results lay the foundation for better understanding the interfacial geochemical processes governing polyP transformation in soil and sediment environments and show the significance for the interpretation of P bioavailability in aquatic environments. Future studies are warranted to explore the effects of other common environmental minerals and solution conditions (e.g., freshwater vs seawater), as well as comparison between abiotic (e.g., mineral catalyzed) vs biotic (e.g., phosphatase enzyme) processes mediated polyP hydrolysis rates, in order to better understand the processes governing the fate of polyP under varied and complex environmental settings.

ASSOCIATED CONTENT

Supporting Information

The Supporting Information is available free of charge on the ACS Publications website at DOI: 10.1021/acsearthspacechem.9b00220.

Texts for characterizations of P compounds and Mn oxides, synthesis of P XAS reference standard, and Mn K-edge XAS analysis; Tables for first-order kinetics fitting parameters and P XANES spectra LCF results; Figures for polyP′ solution and solid NMR spectra, XRD of Mn oxides, plots of total P and metal concentrations, ^{31}P solution NMR spectra of P_3 and Ca-polyP granule supernatants, orthophosphate adsorption isotherm, and Mn XANES spectra and LCF results (PDF)

DOI: 10.1021/acsearthspacechem.9b00220
ACS Earth Space Chem. 2019, 3, 2623−2634

AUTHOR INFORMATION

Corresponding Author

*E-mail: yuanzhi.tang@eas.gatech.edu. Phone: 404-894-3814.

ORCID

Yuanzhi Tang: 0000-0002-7741-8646

Present Address

#J.M.D.: Geosciences Research Division, Scripps Institution of Oceanography, University of California San Diego, La Jolla, CA 92093, United States.

Notes

The authors declare no competing financial interest.

ACKNOWLEDGMENTS

This work was supported by the US National Science Foundation (NSF) under Grants # 1559087, 1710285, 1739884, and 1559124. B.W. thanks the financial support from China Scholarship Council (CSC) under Grant # 201606760059. We acknowledge beamline scientists Erik Nelson (SSRL Beamline 14-3) and Qing Ma (APS Beamline 5-BM-D) for help with XAS experimental setup. Portions of this research were conducted at the Advanced Photon Source (APS) and Stanford Synchrotron Radiation Lightsource (SSRL). APS is a U.S. Department of Energy (DOE) Office of Science User Facility operated for the DOE Office of Science by Argonne National Laboratory under Contract No. DE-AC02-06CH11357. Use of the Stanford Synchrotron Radiation Lightsource, SLAC National Accelerator Laboratory, is supported by the U.S. Department of Energy, Office of Science, Office of Basic Energy Sciences under Contract No. DE-AC02-76SF00515.

REFERENCES

(1) Arai, Y.; Sparks, D. L. Phosphate reaction dynamics in soils and soil components: A multiscale approach. In *Advances in Agronomy*; Donald, L. S., Ed.; Academic Press, 2007; Vol. *94*, pp 135−179.

(2) Ruttenberg, K. C. The global phosphorus cycle. In *Treatise on Geochemistry*, 2nd ed.; Turekian, K. K., Ed.; Elsevier: Oxford, 2014; pp 499−558.

(3) Kornberg, A.; Rao, N. N.; Ault-Riche, D. Inorganic polyphosphate: A molecule of many functions. *Annu. Rev. Biochem.* **1999**, *68*, 89−125.

(4) Azevedo, C.; Saiardi, A. Functions of inorganic polyphosphates in eukaryotic cells: A coat of many colours. *Biochem. Soc. Trans.* **2014**, *42*, 98−102.

(5) Diaz, J. M.; Ingall, E. D. Fluorometric quantification of natural inorganic polyphosphate. *Environ. Sci. Technol.* **2010**, *44* (12), 4665−4671.

(6) Rao, N. N.; Gómez-García, M. R.; Kornberg, A. Inorganic polyphosphate: Essential for growth and survival. *Annu. Rev. Biochem.* **2009**, *78* (1), 605−647.

(7) Paytan, A.; Cade-Menun, B. J.; McLaughlin, K.; Faul, K. L. Selective phosphorus regeneration of sinking marine particles: Evidence from ^{31}P-NMR. *Mar. Chem.* **2003**, *82* (1−2), 55−70.

(8) Martin, P.; Dyhrman, S. T.; Lomas, M. W.; Poulton, N. J.; Van Mooy, B. A. S. Accumulation and enhanced cycling of polyphosphate by Sargasso Sea plankton in response to low phosphorus. *Proc. Natl. Acad. Sci. U. S. A.* **2014**, *111* (22), 8089−8094.

(9) Sannigrahi, P.; Ingall, E. Polyphosphates as a source of enhanced P fluxes in marine sediments overlain by anoxic waters: Evidence from ^{31}P NMR. *Geochem. Trans.* **2005**, *6* (3), 52.

(10) Hupfer, M.; Ruübe, B.; Schmieder, P. Origin and diagenesis of polyphosphate in lake sediments: A ^{31}P-NMR study. *Limnol. Oceanogr.* **2004**, *49* (1), 1−10.

(11) Ebuele, V. O.; Santoro, A.; Thoss, V. Phosphorus speciation by ^{31}P NMR spectroscopy in bracken (*Pteridium aquilinum* (L.) Kuhn) and bluebell (*Hyacinthoides non-scripta* (L.) Chouard ex Rothm.) dominated semi-natural upland soil. *Sci. Total Environ.* **2016**, *566−567*, 1318−1328.

(12) Diaz, J.; Ingall, E.; Benitez-Nelson, C.; Paterson, D.; de Jonge, M. D.; McNulty, I.; Brandes, J. A. Marine polyphosphate: A key player in geologic phosphorus sequestration. *Science* **2008**, *320* (5876), 652−5.

(13) Brandes, J. A.; Ingall, E.; Paterson, D. Characterization of minerals and organic phosphorus species in marine sediments using soft X-ray fluorescence spectromicroscopy. *Mar. Chem.* **2007**, *103* (3−4), 250−265.

(14) Kulakovskaya, T. V.; Vagabov, V. M.; Kulaev, I. S. Inorganic polyphosphate in industry, agriculture and medicine: Modern state and outlook. *Process Biochem.* **2012**, *47* (1), 1−10.

(15) Martin, P.; Lauro, F. M.; Sarkar, A.; Goodkin, N.; Prakash, S.; Vinayachandran, P. N. Particulate polyphosphate and alkaline phosphatase activity across a latitudinal transect in the tropical Indian Ocean. *Limnol. Oceanogr.* **2018**, *63* (3), 1395−1406.

(16) Miller, A. P.; Arai, Y. Investigation of acid hydrolysis reactions of polyphosphates and phytic acid in Bray and Mehlich III extracting solutions. *Biol. Fertil. Soils* **2017**, *53* (7), 737−742.

(17) de Jager, H. J.; Heyns, A. M. Kinetics of acid-catalyzed hydrolysis of a polyphosphate in water. *J. Phys. Chem. A* **1998**, *102* (17), 2838−2841.

(18) Kura, G. Alkaline hydrolysis of inorganic *cyclo*-polyphosphates. *Bull. Chem. Soc. Jpn.* **1987**, *60* (8), 2857−2860.

(19) Huang, R.; Wan, B.; Hultz, M.; Diaz, J. M.; Tang, Y. Phosphatase-mediated hydrolysis of linear polyphosphates. *Environ. Sci. Technol.* **2018**, *52* (3), 1183−1190.

(20) Hamilton, J. G.; Hilger, D.; Peak, D. Mechanisms of tripolyphosphate adsorption and hydrolysis on goethite. *J. Colloid Interface Sci.* **2017**, *491*, 190−198.

(21) Wan, B.; Huang, R.; Diaz, J. M.; Tang, Y. Polyphosphate adsorption and hydrolysis on aluminum oxides. *Environ. Sci. Technol.* **2019**, *53* (16), 9542−9552.

(22) Inman, M. P.; Beattie, J. K.; Jones, D. R.; Baldwin, D. S. Abiotic hydrolysis of the detergent builder tripolyphosphate by hydrous manganese dioxide. *Water Res.* **2001**, *35* (8), 1987−1993.

(23) Li, W.; Xu, W.; Parise, J. B.; Phillips, B. L. Formation of hydroxylapatite from co-sorption of phosphate and calcium by boehmite. *Geochim. Cosmochim. Acta* **2012**, *85*, 289−301.

(24) Huang, J.; Zhong, S.; Dai, Y.; Liu, C.-C.; Zhang, H. Effect of MnO_2 phase structure on the oxidative reactivity toward bisphenol A degradation. *Environ. Sci. Technol.* **2018**, *52* (19), 11309−11318.

(25) Zhao, S.; Wang, Q.; Sun, J.; Borkiewicz, O. J.; Huang, R.; Saad, E. M.; Fields, B.; Chen, S.; Zhu, M.; Tang, Y. Effect of Zn coprecipitation on the structure of layered Mn oxides. *Chem. Geol.* **2018**, *493*, 234−245.

(26) Meng, Y.; Song, W.; Huang, H.; Ren, Z.; Chen, S.-Y.; Suib, S. L. Structure−property relationship of bifunctional MnO_2 nanostructures: Highly efficient, ultra-Stable electrochemical water oxidation and oxygen reduction reaction catalysts identified in alkaline media. *J. Am. Chem. Soc.* **2014**, *136* (32), 11452−11464.

(27) Murphy, J.; Riley, J. P. A modified single solution method for the determination of phosphate in natural waters. *Anal. Chim. Acta* **1962**, *27*, 31−36.

(28) Das, P.; Metcalfe, C. D.; Xenopoulos, M. A. Interactive effects of silver nanoparticles and phosphorus on phytoplankton growth in natural waters. *Environ. Sci. Technol.* **2014**, *48* (8), 4573−4580.

(29) Huang, R. X.; Tang, Y. Z. Evolution of phosphorus complexation and mineralogy during (hydro) thermal treatments of activated and anaerobically digested sludge: Insights from sequential extraction and P K-edge XANES. *Water Res.* **2016**, *100*, 439−447.

(30) Ravel, á.; Newville, M. ATHENA, ARTEMIS, HEPHAESTUS: Data analysis for X-ray absorption spectroscopy using IFEFFIT. *J. Synchrotron Radiat.* **2005**, *12* (4), 537−541.

DOI: 10.1021/acsearthspacechem.9b00220
ACS Earth Space Chem. 2019, 3, 2623−2634

(31) Baldwin, D. S.; Beattie, J. K.; Coleman, L. M.; Jones, D. R. Phosphate ester hydrolysis facilitated by mineral phases. *Environ. Sci. Technol.* **1995**, *29* (6), 1706−1709.
(32) Yan, Y. P.; Liu, F.; Li, W.; Liu, F.; Feng, X. H.; Sparks, D. L. Sorption and desorption characteristics of organic phosphates of different structures on aluminium (oxyhydr)oxides. *Eur. J. Soil Sci.* **2014**, *65* (2), 308−317.
(33) Wan, B.; Yan, Y. P.; Zhu, M. Q.; Wang, X. M.; Liu, F.; Tan, W. F.; Feng, X. H. Quantitative and spectroscopic investigations of the co-sorption of *myo*-inositol hexakisphosphate and cadmium(II) on to haematite. *Eur. J. Soil Sci.* **2017**, *68* (3), 374−383.
(34) Maki, H.; Tsujito, M.; Sakurai, M.; Yamada, T.; Nariai, H.; Mizuhata, M. Stabilities of the divalent metal ion complexes of a short-chain polyphosphate anion and its imino derivative. *J. Solution Chem.* **2013**, *42* (11), 2104−2118.
(35) Sigel, H. Interactions of metal ions with nucleotides and nucleic acids and their constituents. *Chem. Soc. Rev.* **1993**, *22* (4), 255−267.
(36) Bunker, B. C.; Arnold, G. W.; Wilder, J. A. Phosphate glass dissolution in aqueous solutions. *J. Non-Cryst. Solids* **1984**, *64* (3), 291−316.
(37) Ingall, E. D.; Brandes, J. A.; Diaz, J. M.; de Jonge, M. D.; Paterson, D.; McNulty, I.; Elliott, W. C.; Northrup, P. Phosphorus K-edge XANES spectroscopy of mineral standards. *J. Synchrotron Radiat.* **2011**, *18* (2), 189−197.
(38) Ramstedt, M.; Norgren, C.; Shchukarev, A.; Sjöberg, S.; Persson, P. Co-adsorption of cadmium(II) and glyphosate at the water−Manganite (γ-MnOOH) interface. *J. Colloid Interface Sci.* **2005**, *285* (2), 493−501.
(39) Zaman, M. I.; Mustafa, S.; Khan, S.; Xing, B. Effect of phosphate complexation on Cd^{2+} sorption by manganese dioxide (β-MnO_2). *J. Colloid Interface Sci.* **2009**, *330* (1), 9−19.
(40) Wang, Q.; Liao, X.; Xu, W.; Ren, Y.; Livi, K. J.; Zhu, M. Synthesis of birnessite in the presence of phosphate, silicate, or sulfate. *Inorg. Chem.* **2016**, *55* (20), 10248−10258.
(41) Prietzel, J.; Harrington, G.; Hausler, W.; Heister, K.; Werner, F.; Klysubun, W. Reference spectra of important adsorbed organic and inorganic phosphate binding forms for soil P speciation using synchrotron-based K-edge XANES spectroscopy. *J. Synchrotron Radiat.* **2016**, *23* (2), 532−544.
(42) Coleman, J. E. Structure and mechanism of alkaline phosphatase. *Annu. Rev. Biophys. Biomol. Struct.* **1992**, *21* (1), 441−483.
(43) Schenk, G.; Elliott, T. W.; Leung, E.; Carrington, L. E.; Mitić, N.; Gahan, L. R.; Guddat, L. W. Crystal structures of a purple acid phosphatase, representing different steps of this enzyme's catalytic cycle. *BMC Struct. Biol.* **2008**, *8* (1), 6.
(44) Schenk, G.; Mitić, N.; Gahan, L. R.; Ollis, D. L.; McGeary, R. P.; Guddat, L. W. Binuclear metallohydrolases: Complex mechanistic strategies for a simple chemical reaction. *Acc. Chem. Res.* **2012**, *45* (9), 1593−1603.
(45) Williams, N. H.; Takasaki, B.; Wall, M.; Chin, J. Structure and nuclease activity of simple dinuclear metal complexes: Quantitative dissection of the role of metal ions. *Acc. Chem. Res.* **1999**, *32* (6), 485−493.
(46) Zhao, H.; Dong, Y.; Jiang, P.; Wang, G.; Zhang, J.; Li, K.; Feng, C. An α-MnO_2 nanotube used as a novel catalyst in ozonation: Performance and the mechanism. *New J. Chem.* **2014**, *38* (4), 1743−1750.
(47) Allard, S.; Gallard, H. Abiotic formation of methyl iodide on synthetic birnessite: A mechanistic study. *Sci. Total Environ.* **2013**, *463*−*464*, 169−175.
(48) Tan, F.; Zhang, Y.; Wang, J.; Wei, J.; Cai, Y.; Qian, X. An efficient method for dephosphorylation of phosphopeptides by cerium oxide. *J. Mass Spectrom.* **2008**, *43* (5), 628−632.
(49) Mäkie, P.; Persson, P.; Österlund, L. Adsorption of trimethyl phosphate and triethyl phosphate on dry and water pre-covered hematite, maghemite, and goethite nanoparticles. *J. Colloid Interface Sci.* **2013**, *392*, 349−358.
(50) Hou, J.; Li, Y.; Liu, L.; Ren, L.; Zhao, X. Effect of giant oxygen vacancy defects on the catalytic oxidation of OMS-2 nanorods. *J. Mater. Chem. A* **2013**, *1* (23), 6736−6741.
(51) Cheng, F.; Zhang, T.; Zhang, Y.; Du, J.; Han, X.; Chen, J. Enhancing electrocatalytic oxygen reduction on MnO_2 with vacancies. *Angew. Chem., Int. Ed.* **2013**, *52* (9), 2474−2477.
(52) Hou, J.; Li, Y.; Mao, M.; Ren, L.; Zhao, X. Tremendous effect of the morphology of birnessite-type manganese oxide nanostructures on catalytic activity. *ACS Appl. Mater. Interfaces* **2014**, *6* (17), 14981−14987.
(53) Liu, R.; Liu, H.; Qiang, Z.; Qu, J.; Li, G.; Wang, D. Effects of calcium ions on surface characteristics and adsorptive properties of hydrous manganese dioxide. *J. Colloid Interface Sci.* **2009**, *331* (2), 275−280.
(54) Kwon, K. D.; Refson, K.; Sposito, G. Understanding the trends in transition metal sorption by vacancy sites in birnessite. *Geochim. Cosmochim. Acta* **2013**, *101*, 222−232.
(55) Zhao, H.; Zhu, M.; Li, W.; Elzinga, E. J.; Villalobos, M.; Liu, F.; Zhang, J.; Feng, X.; Sparks, D. L. Redox reactions between Mn(II) and hexagonal birnessite change its layer symmetry. *Environ. Sci. Technol.* **2016**, *50* (4), 1750−1758.
(56) Luo, J.; Meng, X.; Crittenden, J.; Qu, J.; Hu, C.; Liu, H.; Peng, P. Arsenic adsorption on α-MnO_2 nanofibers and the significance of (100) facet as compared with (110). *Chem. Eng. J.* **2018**, *331*, 492−500.
(57) Cooper, D. C.; Picardal, F. F.; Coby, A. J. Interactions between microbial iron reduction and metal geochemistry: Effect of redox cycling on transition metal speciation in iron bearing sediments. *Environ. Sci. Technol.* **2006**, *40* (6), 1884−1891.
(58) Müller, B.; Granina, L.; Schaller, T.; Ulrich, A.; Wehrli, B. P, As, Sb, Mo, and other elements in sedimentary Fe/Mn layers of lake Baikal. *Environ. Sci. Technol.* **2002**, *36* (3), 411−420.
(59) Worsfold, P. J.; Monbet, P.; Tappin, A. D.; Fitzsimons, M. F.; Stiles, D. A.; McKelvie, I. D. Characterisation and quantification of organic phosphorus and organic nitrogen components in aquatic systems: A Review. *Anal. Chim. Acta* **2008**, *624* (1), 37−58.

DOI: 10.1021/acsearthspacechem.9b00220
ACS Earth Space Chem. 2019, 3, 2623−2634